

EFFICIENT ASYMPTOTIC MODELS FOR AXISYMMETRIC EDDY CURRENT PROBLEMS IN LINEAR FERROMAGNETIC MATERIALS

DIMA ABOU EL NASSER EL YAFI, VICTOR PÉRON

ABSTRACT. The problem under consideration is that of time-harmonic eddy current problems in linear ferromagnetic materials surrounded by a dielectric medium with a smooth common interface. Assuming axisymmetric geometries and orthoradial axisymmetric data, we construct an efficient multiscale expansion for the orthoradial solution that provides reduced computational costs. We investigate numerically the accuracy of the approach using an analytical procedure and infinite cylinders as well. It results that the computation of two asymptotics is sufficient to ensure accurate solutions in the case of low frequencies.

Keywords. Multiscale expansion; Eddy current problems; Analytical method; Ferromagnetic materials; Axisymmetric geometry

1. INTRODUCTION

Eddy currents arise due to the time varying magnetic field crossing metals [6]. The distribution of the current density in this case is restricted at a boundary layer near the metallic surface, and diminishes exponentially inside the conducting medium. This phenomenon is called the *skin effect* [33, 35, 26, 7, 10]. Eddy currents generate energy losses that have two sided effect in the industrial field [32]. On the one hand, these currents can have a good use such as induction heating or for the design of electromagnetic breaking systems. On the other hand, eddy currents can also produce "undesirable" power losses in the form of heating for example which can affect the performance of some electrical devices. Summing up, studying eddy currents is crucial for engineering applications in electromagnetism.

The mathematical and numerical analysis of the eddy current problems have been the interest of many works during the past decades [25, 22, 6, 8, 20, 12, 7, 4, 32]. Because of the small skin depth inside the conductors, the classical numerical methods are challenging to apply. To overcome this difficulty, it is possible to develop an asymptotic method that derives approximate models with less computational costs. The asymptotic approach is often employed for physical problems involving a small or large parameter. This method gives an accurate approximation of the problem by solving an ordered sequence of subproblems independent of the latter parameter.

We refer the reader to [33, 18, 25, 17, 14, 10, 31, 34, 29, 21] for previous works devoting to the asymptotic procedure in electromagnetic problems.

For example, in [18, 25] authors investigated eddy current problems in the case of metals having infinite conductivity by applying first a boundary integral procedure and then an asymptotic procedure that reflects the skin effect in metals in both bi-dimensional and three-dimensional domains. Moreover, recent studies [17, 14, 10] analyzed theoretically and numerically the electromagnetic field solution for the Maxwell equations through an asymptotic expansion for large conductivities. It is worthwhile to note that these previous works tackle the equations of electromagnetism set on a domain made of a dielectric and a non-magnetic conducting subdomains with a smooth common interface. On the other hand, several works have investigated the asymptotic approach for eddy current problems in a bi-dimensional setting where the conducting medium is non-magnetic and has a corner singularity on the conductor-dielectric interface [9, 13, 16]. These works have shown that the asymptotic approach was strongly affected by adding corrections, especially near corners, in order to obtain accurate asymptotic models.

This paper continues a study begun in [30] and [2] of the time harmonic eddy current problems in linear ferromagnetic materials with a smooth interface. The work in [30] was restricted for the theoretical results whereas in [2] was concerned essentially with numerical validation of the asymptotic procedure employed in [30]. In both cases, the study was restricted to a very special class of two-dimensional problems using a multiscale expansion. Besides, [2] is not a straightforward application of [30]. More precisely, we identified in [2] efficient asymptotic models, slightly different than those established in [30], that provide reduced computational costs in time and memory allocation for a wide range of physical parameters. This present work treats a three-dimensional situation in axisymmetric geometry.

However, three dimensional computations can be very expensive. In a number of cases, it is possible to reduce the problem by assuming that the geometry is invariant by translation or rotation [5, 3, 10, 11]. In this context, we choose to consider a special class of axisymmetric geometry that reduces our problem to a one-dimensional scalar model. Our analysis is twofold. First, we present elements of derivation for the multiscale expansion of the one-dimensional solution near the conductor-insulator interface. We identify efficient asymptotic models that reduce the computational costs. Then, we evaluate the performance of the resulting models by presenting numerical results.

In this work we assess the performance of our efficient asymptotic models analytically in the case of infinite cylinders. Indeed, our analytical procedure follows the spirit of [4] where authors tackled eddy current problems for large conductivities and for the case of infinite cylinders as well. There are many differences between our paper and [4]. For example, in [4] authors analyze the performance of the finite element method (FEM) applied to the considered eddy current problems. However, our numerical study is based on analytical methods in order to highlight the good accuracy of our asymptotic approach, for an example of unbounded domain. Actually, the FEM

was previously applied for the eddy current problems in linear ferromagnetic materials [2] where their analytical solution was not obvious to calculate because of the complexity of the considered bounded geometry. Moreover, in [4], authors considered infinite cylinders, in width and length, consisting of a core material surrounded by a crucible and an extremely thin coil. The crucible itself is made of several concentric layers with different materials. In our case, for the sake of simplicity, we consider only two different layers: a ferromagnetic material surrounded by a dielectric material with a common smooth interface. Finally, we perform numerically a comparison of our asymptotic approach with the impedance method [23, 17].

The presentation of the paper proceeds as follows. Section 2 introduces the framework as well as the boundary value problem. In section 3, we restrict our work to axisymmetric domains and orthoradial axisymmetric data. Moreover, we apply in the latter section a multiscale expansion for the orthoradial component of the magnetic vector potential and we identify efficient asymptotic models up to the order two. In section 5, we present numerical results to assess the performance of the proposed models. Concluding remarks and perspectives are given in section 6. In appendix A, we provide elements of proof of the multiscale expansion given in the subsection 3.3. Appendix B is dedicated to a deep calculation of the analytical solutions introduced in the section 4.

2. PROBLEM SETTING

Throughout the paper we denote by $\Omega \subset \mathbb{R}^3$ a smooth and connected domain with boundary Γ , and Ω_- a smooth connected subdomain of Ω with boundary Σ . We denote by Ω_0 the complementary of $\overline{\Omega_-}$, see for instance Figure 1.

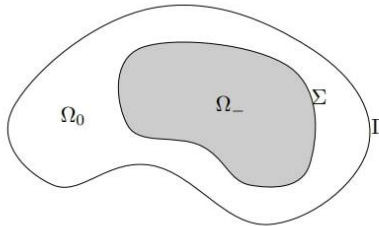


FIGURE 1. A cross section of the domain Ω and its subdomains Ω_- , Ω_0

2.1. Notations and physical parameters. We suppose that Ω_0 is a dielectric medium which we consider for the sake of simplicity the free space, and Ω_- is a ferromagnetic material. The magnetic permeability and the

conductivity are given by the following piecewise-constant functions $\underline{\mu}$ and $\underline{\sigma}$ respectively:

$$(1) \quad \underline{\mu} = \begin{cases} \mu_0 & \text{in } \Omega_0 \\ \mu_r \mu_0 & \text{in } \Omega_- \end{cases} \quad \text{and} \quad \underline{\sigma} = \begin{cases} 0 & \text{in } \Omega_0 \\ \sigma > 0 & \text{in } \Omega_-, \end{cases}$$

where $\mu_0 = 4\pi \times 10^{-7}$ [H/m](henry per meter) and the relative permeability μ_r is assumed to be a large parameter. The angular frequency is denoted by $\omega > 0$. In our work, ω and σ are given parameters. We denote by J_s the current source which is supposed for the sake of simplicity divergence free that is $\text{div } J_s = 0$ in Ω , smooth enough and the support of J_s does not meet Ω_- . We consider the following notations.

Notation 1. We denote by h^+ (resp. h^-) the restriction of any function h in Ω_0 (resp. Ω_-).

Notation 2. In order to introduce our asymptotic method, we define a small parameter ε as follows

$$\varepsilon = \frac{1}{\mu_r \delta},$$

where δ is the skin depth and given by

$$\delta = \sqrt{\frac{2}{\omega \sigma \mu_r \mu_0}}.$$

2.2. Boundary value problem. The magnetic vector potential $\mathcal{A} = (\mathcal{A}^+, \mathcal{A}^-)$ satisfies the following boundary value problem [15]

$$(2) \quad \left\{ \begin{array}{ll} \text{curl curl } \mathcal{A}^+ = \mu_0 J_s & \text{in } \Omega_0, \\ \text{curl curl } \mathcal{A}^- - i \omega \sigma \mu_0 \mu_r \mathcal{A}^- = 0 & \text{in } \Omega_-, \\ \text{div } \mathcal{A}^- = 0 & \text{in } \Omega_-, \\ \mathcal{A}^+ \times n = \mathcal{A}^- \times n & \text{on } \Sigma, \\ \text{curl } \mathcal{A}^+ \times n = \mu_r^{-1}(\text{curl } \mathcal{A}^- \times n) & \text{on } \Sigma, \\ \mathcal{A}^- \cdot n = 0 & \text{on } \Sigma, \\ \mathcal{A}^+ \times n = 0 & \text{on } \Gamma. \end{array} \right. \iff \left\{ \begin{array}{ll} \text{curl curl } \mathcal{A}^+ = \mu_0 J_s & \text{in } \Omega_0, \\ \text{curl curl } \mathcal{A}^- - 2i\delta^{-2} \mathcal{A}^- = 0 & \text{in } \Omega_-, \\ \text{div } \mathcal{A}^- = 0 & \text{in } \Omega_-, \\ \mathcal{A}^+ \times n = \mathcal{A}^- \times n & \text{on } \Sigma, \\ \text{curl } \mathcal{A}^+ \times n = \delta \varepsilon (\text{curl } \mathcal{A}^- \times n) & \text{on } \Sigma, \\ \mathcal{A}^- \cdot n = 0 & \text{on } \Sigma, \\ \mathcal{A}^+ \times n = 0 & \text{on } \Gamma. \end{array} \right.$$

This problem has to be completed by the gauge conditions [8, 20, 12, 29]

$$(3) \quad \text{div } \mathcal{A}^+ = 0 \text{ in } \Omega_0 \quad \text{and} \quad \int_{\Sigma} \mathcal{A}^+ \cdot n \, dS = 0.$$

For numerical purposes, we used here the modified magnetic vector potential [15, section 4.4 - page 25], so its boundary value problem (2) is deduced from that of the electric field.

2.3. Variational formulation. We define the following space

$$(4) \quad \mathbf{H}_0(\text{curl}, \Omega) = \{u \in \mathbf{L}^2(\Omega) \mid \text{curl } u \in \mathbf{L}^2(\Omega), u \times n = 0 \text{ on } \Gamma\}.$$

The variational space is the Hilbert space \mathbf{Y} :

$$(5) \quad \mathbf{Y} = \{u \in \mathbf{H}_0(\text{curl}, \Omega) \mid \text{div } u^+ \in L^2(\Omega_0), \text{div } u^- \in L^2(\Omega_-), \int_{\Sigma} u^+ \cdot n \, dS = 0\}$$

endowed with the norm

$$\|u\|_{\mathbf{Y}}^2 = \|u\|_{0,\Omega}^2 + \|\text{curl } u\|_{0,\Omega}^2 + \|\text{div } u^+\|_{0,\Omega_0}^2 + \|\text{div } u^-\|_{0,\Omega_-}^2.$$

We introduce the small parameter $\nu = \frac{1}{\sqrt{\mu_r}}$ in the problem below. For all $\nu > 0$, the variational problem writes

Find $\mathcal{A} \in \mathbf{Y}$ such that for all $v \in \mathbf{Y}$,

$$(6) \quad a_R(\mathcal{A}, v) = \mu_0 \int_{\Omega} J_s \cdot \bar{v} \, dx.$$

Here the sesquilinear form in its regularized version a_R is defined as [12, 29]

$$\begin{aligned} a_R(u, v) &= \nu^2 \int_{\Omega_-} \text{curl } u^- \cdot \text{curl } \bar{v}^- \, dx + \int_{\Omega_0} \text{curl } u^+ \cdot \text{curl } \bar{v}^+ \, dx + \int_{\Omega_0} \text{div } u^+ \text{div } \bar{v}^+ \, dx \\ &\quad + \int_{\Omega_-} \text{div } u^- \text{div } \bar{v}^- \, dx - i\omega\sigma\mu_0 \int_{\Omega_-} u^- \cdot \bar{v}^- \, dx. \end{aligned}$$

In the following, we will study numerically the time-harmonic eddy current problems in axisymmetric geometry which can represent correctly the features of our three dimensional problem.

3. AXISYMMETRIC DOMAINS

In this section, we choose to consider similar framework and notations introduced in [10, section 4] in the case of axisymmetric domains and axisymmetric orthoradial data. We suppose that Ω_0 and Ω_- are axisymmetric domains with the same axis of rotation denoted by E_0 which coincides with the z -axis. In this case, there exists bi-dimensional "meridian" domains Ω^m , Ω_0^m , and Ω_-^m satisfying, in cylindrical coordinates (r, θ, z) , the following assumptions

$$(7) \quad \begin{aligned} \Omega &= \{x \in \mathbb{R}^3 / (r, z) \in \Omega^m, \theta \in \mathbb{T}\}, \\ \Omega_0 &= \{x \in \mathbb{R}^3 / (r, z) \in \Omega_0^m, \theta \in \mathbb{T}\}, \\ \Omega_- &= \{x \in \mathbb{R}^3 / (r, z) \in \Omega_-^m, \theta \in \mathbb{T}\}. \end{aligned}$$

Here $\mathbb{T} = \mathbb{R}/(2\pi\mathbb{Z})$ is the one dimensional torus. In Figure 2, Γ^m and Σ^m are the meridian curves corresponding to Γ and Σ , and Γ_0, Γ_0^+ are the following subsets of the rotation axis E_0

$$\Gamma_0 = E_0 \cap \overline{\Omega^m} \quad \text{and} \quad \Gamma_0^+ = E_0 \cap \overline{\Omega_0^m}.$$

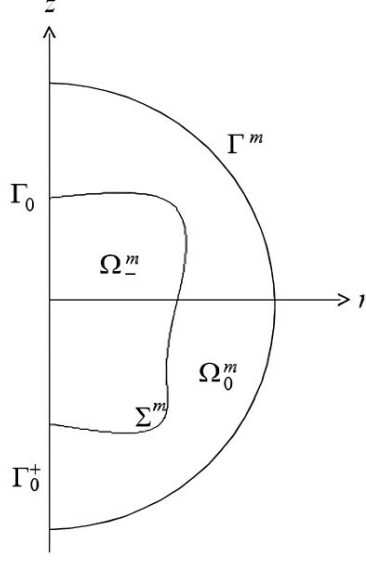


FIGURE 2. The meridian domain $\Omega = \Omega_-^m \cup \Omega_0^m \cup \Sigma^m$ with boundary $\partial\Omega^m = \Gamma^m \cup \Gamma_0$

3.1. Formulation in cylindrical coordinates. In this part, we recall the cylindrical coordinates of a vector field \mathcal{A} and the curl operator:

- For a vector field $\mathcal{A} = (\mathcal{A}_1, \mathcal{A}_2, \mathcal{A}_3)$ we denote by (A_r, A_θ, A_z) its cylindrical components such that

$$\begin{cases} A_r(r, \theta, z) = \mathcal{A}_1(x) \cos \theta + \mathcal{A}_2(x) \sin \theta, \\ A_\theta(r, \theta, z) = -\mathcal{A}_1(x) \sin \theta + \mathcal{A}_2(x) \cos \theta, \\ A_z(r, \theta, z) = \mathcal{A}_3(x), \end{cases}$$

and we set $\hat{\mathcal{A}}(r, \theta, z) = (A_r(r, \theta, z), A_\theta(r, \theta, z), A_z(r, \theta, z))$.

- The cylindrical components of the curl operator applied to a vector field \mathcal{A} writes

$$(8) \quad \begin{cases} (\text{curl } \mathcal{A})_r = \frac{1}{r} \partial_\theta A_z - \partial_z A_\theta, \\ (\text{curl } \mathcal{A})_\theta = \partial_z A_r - \partial_r A_z, \\ (\text{curl } \mathcal{A})_z = \frac{1}{z} \partial_r (r A_\theta), \end{cases}$$

and the divergence operator div writes

$$(9) \quad \text{div } \mathcal{A} = \partial_r A_r + \frac{1}{r} A_r + \frac{1}{r} \partial_\theta A_\theta + \partial_z A_z.$$

3.2. Axisymmetric orthoradial problem.

3.2.1. Preliminaries. For a vector field $\mathcal{A} = (\mathcal{A}_1, \mathcal{A}_2, \mathcal{A}_3)$, we say that

- \mathcal{A} is **axisymmetric** if $\hat{\mathcal{A}}$ does not depend on the angular variable θ .
- \mathcal{A} is **orthoradial** if its components A_r and A_z are equal to zero.

On our axisymmetric configuration, we consider a modification of problem (2) [10]: We take $J_s = 0$ and impose instead a non-homogeneous boundary condition

$$(10) \quad \mathcal{A} \times n = G \times n \quad \text{on } \Gamma,$$

for a given smooth data G .

Assumption 1. *We assume that G is axisymmetric and orthoradial i.e.*

$$(11) \quad \hat{G}(r, \theta, z) = (0, g_\theta(r, z), 0).$$

Under Assumption 1, it results that \mathcal{A} is also axisymmetric and orthoradial

$$(12) \quad \hat{\mathcal{A}}(r, \theta, z) = (0, A_\theta(r, z), 0),$$

see for instance [10, 28] for the proof of similar works.

In that follows, we will drop the notation θ in A_θ , and we will concentrate our asymptotic analysis on this orthoradial component. For the sake of clarity, we consider the following notations.

Notation 3. *We denote by (n_1, n_2, n_3) the cartesian coordinates of the unit normal vector n on Σ inwardly oriented to Ω_- . Since Ω_- is an axisymmetric domain, then it results that $n_\theta = 0$ and the unit normal vector in cylindrical coordinates writes $\hat{n} = (n_r, 0, n_z)$ [28, page 166]. Considering an axisymmetric and orthoradial solution (12), we introduce then the orthoradial component of the curlcurl operator and the boundary operator $\text{curl} \times n$ respectively as follows:*

$$(13) \quad \begin{aligned} D(r, z; \partial_r, \partial_z) &= \partial_r^2 + \frac{1}{r} \partial_r + \partial_z^2 - \frac{1}{r^2}, \\ B(r, z; \partial_r, \partial_z) &= n_r (\partial_r + \frac{1}{r}) + n_z \partial_z, \end{aligned}$$

and the divergence operator is free in this case, see for instance (9).

3.2.2. Variational problem. By using the change of variables from cartesian to cylindrical coordinates, we associate the following weighted Sobolev space in order to define the orthoradial component $A(r, z)$ [5, 10]

$$V_{1, \Gamma^m}^1(\Omega^m) = \{u \in H_1^1(\Omega^m) \mid u \in L_{-1}^2(\Omega^m) \text{ and } u = 0 \text{ on } \Gamma^m\}.$$

Here,

$$H_1^1(\Omega^m) = \{u \in L_1^2(\Omega^m) \mid \partial_r^j \partial_z^{1-j} u \in L_1^2(\Omega^m), j = 0, 1\},$$

and for all $\alpha \in \mathbb{R}$, the space $L_\alpha^2(\Omega^m)$ is the set of measurable functions $u(r, z)$ such that

$$(14) \quad \|u\|_{L_\alpha^2(\Omega^m)}^2 = \int_{\Omega^m} |u|^2 r^\alpha dr dz < +\infty.$$

The following remark incorporates an essential boundary condition.

Remark 1. *All functions on V_{1, Γ^m}^1 have null trace on Γ_0 , see [5, Remark II.1.1], and [10, Remark 4.1] for more details about the proof.*

As a result, we solve the following two-dimensional scalar problem set in Ω^m .

Find $A \in V_{1,\Gamma^m}^1(\Omega^m) + g$ such that for all $v \in V_{1,\Gamma^m}^1(\Omega^m)$,

$$(15) \quad a(A, v) = 0,$$

where

$$\begin{aligned} a(u, v) = & \nu^2 \int_{\Omega_-^m} \left(\partial_z u^- \partial_z \overline{v^-} + \frac{1}{r} \partial_r (r u^-) \frac{1}{r} \partial_r (r \overline{v^-}) \right) r dr dz - i \omega \sigma \mu_0 \int_{\Omega_-^m} u^- \overline{v^-} r dr dz \\ & + \int_{\Omega_0^m} \left(\partial_z u^+ \partial_z \overline{v^+} + \frac{1}{r} \partial_r (r u^+) \frac{1}{r} \partial_r (r \overline{v^+}) \right) r dr dz, \end{aligned}$$

and recalling that $\nu = \frac{1}{\sqrt{\mu_r}}$.

3.2.3. Strong form of equations. According to (13) and Remark 1, the orthoradial component $A = (A^+, A^-)$ satisfies the following problem

$$(16) \quad \begin{cases} DA^+ = 0 & \text{in } \Omega_0^m \\ DA^- - 2i\delta^{-2}A^- = 0 & \text{in } \Omega_-^m \\ BA^+ = \varepsilon\delta BA^- & \text{on } \Sigma^m, \\ A^+ = A^- & \text{on } \Sigma^m, \\ A^+ = g_\theta & \text{on } \Gamma^m \cup \Gamma_0^+, \end{cases}$$

where g_θ is defined in Eq. (11), see for instance [28, Chapter 8] for similar work. Under the assumption of orthoradial and axisymmetric data and from notation 3, we deduce directly that the gauge conditions (3) in the cylindrical coordinates are satisfied.

3.3. Multiscale expansion. In this part, we aim to expand the orthoradial component A of the magnetic vector potential using a multiscale expansion. First, we introduce the following geometrical notations.

Notation 4 (Geometrical setting). We set $\xi \mapsto \tau(\xi) = (r(\xi), z(\xi))$ a \mathcal{C}^∞ function, $\xi \in (0, L)$ be an arc-length coordinate on the interface Σ^m , and L is the length of the curve Σ^m . Let (ξ, h) be the associate normal coordinate system in a tubular neighborhood \mathcal{U}_-^m of Σ^m inside Ω_-^m (see for instance Figure 12). Then the normal vector $n(\xi)$ at the point $\tau(\xi)$ can be written as (Frenet frame)

$$(17) \quad n(\xi) = (-z'(\xi), r'(\xi)),$$

where $z'(\xi) = \frac{dz}{d\xi}$, and $r'(\xi) = \frac{dr}{d\xi}$. Further, we denote by $k(\xi)$ the curvature of Σ^m at $\tau(\xi)$ which is defined as [10]

$$k(\xi) = (r'z'' - z'r'')(\xi).$$

Finally, we set χ a smooth cut-off function with support in $\overline{\mathcal{U}_-^m}$, and equals to 1 in a smaller neighborhood of Σ^m .

Now, we exhibit expansions series for A which we denote by A^+ in the dielectric part Ω_0^m , and by A^- in the conducting part Ω_-^m :

$$(18) \quad \begin{aligned} A^+(r, z) &= A_0^+(r, z) + \frac{\varepsilon}{\hat{\alpha}} A_1^+(r, z) + \mathcal{O}(\varepsilon^2), \\ A^-(r, z) &= A_0^-(r, z; \delta) + \delta A_1^-(r, z; \delta) + \mathcal{O}(\delta^2) \\ &\text{with } A_j^-(r, z; \delta) = \chi(h) \mathfrak{A}_j(\xi, \frac{h}{\delta}). \end{aligned}$$

Here $\hat{\alpha} = \frac{1-i}{2}$ where i is the unit complex number. Besides, the profiles \mathfrak{A}_j are defined on $\Sigma^m \times (0, +\infty)$, and $\mathfrak{A}_j \rightarrow 0$ as $Y_3 = \frac{h}{\delta} \rightarrow +\infty$. The symbol $\mathcal{O}(\varepsilon^2)$ (resp. $\mathcal{O}(\delta^2)$) means that the remainder is uniformly bounded by ε^2 (resp. δ^2). Hereafter, we focus on the first terms A_0^+ , \mathfrak{A}_0 , A_1^+ and \mathfrak{A}_1 .

3.3.1. First terms of the asymptotic expansion: We construct the first asymptotics (A_0^+, \mathfrak{A}_0) and (A_1^+, \mathfrak{A}_1) recursively. Elements of formal derivations are given in appendix A.

First, A_0^+ solves the following problem

$$(19) \quad \begin{cases} DA_0^+ = 0 & \text{in } \Omega_0^m, \\ BA_0^+ = 0 & \text{on } \Sigma^m, \\ A_0^+ = g_\theta & \text{on } \Gamma^m \cup \Gamma_0^+. \end{cases}$$

Then the first profile \mathfrak{A}_0 is defined as follows:

$$(20) \quad \mathfrak{A}_0(\xi, Y_3) = A_0^+(\tau(\xi)) e^{-\frac{Y_3}{\hat{\alpha}}},$$

where $(\xi, Y_3) \in \mathbb{T}_L \times (0, +\infty)$, noting that $\mathbb{T}_L = \mathbb{R}/L\mathbb{Z}$.

The next asymptotic solves the problem below:

$$(21) \quad \begin{cases} DA_1^+ = 0 & \text{in } \Omega_0^m, \\ BA_1^+ = -A_0^+ & \text{on } \Sigma^m, \\ A_1^+ = 0 & \text{on } \Gamma^m \cup \Gamma_0^+. \end{cases}$$

The second profile \mathfrak{A}_1 satisfies the following equality

$$(22) \quad \mathfrak{A}_1(\xi, Y_3) = \left[\frac{1}{\hat{\alpha}\delta_0^2} A_1^+(\tau(\xi)) - \frac{Y_3}{2} \left(k + \frac{z'}{r} \right) (\xi) A_0^+(\tau(\xi)) \right] e^{-\frac{Y_3}{\hat{\alpha}}},$$

where $\delta_0 = \sqrt{\frac{2}{\omega\sigma\mu_0}}$. Similarly to [10, Remark 4.2], we deduce the following remark.

Remark 2. *Subsequently, we assume that g_θ , defined in Eq. (11), is a real valued function. Thus, the right hand side of the boundary value problem (19) is real. Hence, A_0^+ is a real valued function. Similarly, we deduce that A_1^+ is also a real valued function.*

Remark 3. *The models (19) and (21) are independent of any physical parameter introduced in this work, which allow us to approach the solution A of the problem (2) in the dielectric part with minimal time and memory allocation as well. We provided a deep numerical study about the computational costs in the special issue [2] for the bi-dimensional case. We will tackle these issues in a forthcoming work for three-dimensional and axisymmetric geometries.*

3.3.2. *Impedance model.* As a by product of the asymptotic expansion, we get a simpler problem than (2) as follows

$$(23) \quad \begin{cases} DA_1^\varepsilon = 0 & \text{in } \Omega_0^m, \\ BA_1^\varepsilon + \frac{\varepsilon}{\alpha} A_1^\varepsilon = 0 & \text{on } \Sigma^m, \\ A_1^\varepsilon = g_\theta & \text{on } \Gamma^m \cup \Gamma_0^+, \end{cases}$$

where the second condition in (23) is the classical Leontovitch condition, see for instance [23], [30, section 6.4], and [2, section 3.1]. It is well known that the impedance solution has a high accuracy with respect to the solution of the eddy current problems. Accordingly, we will compare numerically our first asymptotic solutions with the latter impedance solution in the next section by using an analytical procedure.

4. RADIAL SOLUTIONS IN CYLINDRICAL GEOMETRY

In that follows, our goal is to provide an analytical study of the considered asymptotic models up to the order two in the dielectric part Ω_0^m . First, we will introduce geometrical and physical assumptions. Then we will give the expressions of the analytical solutions for the global, asymptotic and impedance problems (16), (19), (21) and (23) respectively that are calculated in appendix B. We will assess the accuracy of the resulting asymptotic solutions numerically in the next section.

4.1. **Framework.** We consider a cylindrical geometry: We assume that Ω^m is an infinite cylinder in length consisting of a ferromagnetic material surrounded by a dielectric domain. Let R_1 be the radius of the interior ferromagnetic cylinder and R_2 the radius of the domain Ω^m . Recall that we denote by (r, θ, z) the cylindrical coordinate system where the z -axis coincides with the axis of the cylinders Ω_-^m and Ω^m , and by $(\vec{e}_r, \vec{e}_\theta, \vec{e}_z)$ the local unit vectors in the cylindrical coordinate system. We will assume that the electric current flows in the dielectric domain Ω_0 in the \vec{e}_θ direction and that is uniformly distributed in the \vec{e}_z direction. In order to solve our problem, we impose a Dirichlet condition at $r = R_2$:

$$(24) \quad A^+(r) = \frac{k}{r},$$

where k is a given constant. The geometry is depicted in Figures 3-4 below.

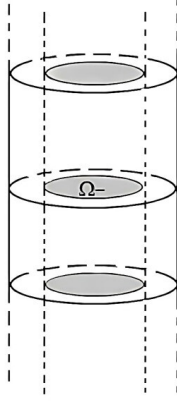


FIGURE 3. Considered geometry

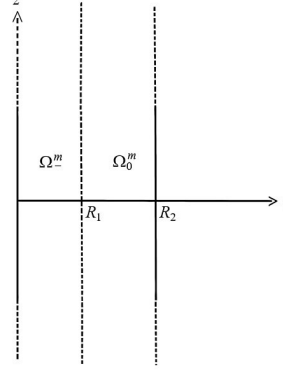


FIGURE 4. The meridional domain Ω^m

4.2. Analytical solutions. In the following part, we will exhibit the analytical expressions of $A = (A^+, A^-)$, A_0^+ , A_1^+ and A_1^\mp solutions of problems (16), (19), (21) and (23) respectively.

4.2.1. *Analytical global solutions.* According to [4, Eq. (A.11)-(A.12)] and appendix B, the general form of the solutions A^+ and A^- are as follows

$$(25) \quad \begin{aligned} A^+(r) &= \frac{r}{2}a + \frac{b}{r}, \\ A^-(r) &= \mathcal{I}_1(\gamma r)c, \end{aligned}$$

where $\gamma = \sqrt{\omega\sigma\mu_r\mu_0}e^{+i\frac{\pi}{4}}$, \mathcal{I}_1 is the modified Bessel function of the first kind [27, Chapter 10 - pages 248–250], and a , b and c are constants deduced from the boundary conditions of the above problem (16) and having the following expressions:

$$\begin{aligned} a &= \frac{k}{R_1} \frac{g_1}{g_2}, \\ b &= k - a \frac{R_2^2}{2}, \\ c &= [\mathcal{I}_1^{-1}(\gamma R_1) \frac{(R_1^2 - R_2^2)}{2R_1}] a + \frac{k}{R_1} \mathcal{I}_1^{-1}(\gamma R_1). \end{aligned}$$

Noting that g_1 and g_2 are constants defined as follows

$$\begin{aligned} g_1 &= \mathcal{I}_1(\gamma R_1) + \gamma R_1 \mathcal{I}_1'(\gamma R_1), \\ g_2 &= R_1 \mu_r \mathcal{I}_1(\gamma R_1) - g_1 \frac{(R_1^2 - R_2^2)}{2R_1}. \end{aligned}$$

4.2.2. *Analytical asymptotic solutions.* We find the analytical expressions of A_0^+ and A_1^+ by a simple integration of the first equations in Ω_0^m of (19) and

(21). The latter asymptotics have the following general form:

$$(26) \quad \begin{aligned} A_0^+(r) &= \frac{r}{2}a_0 + \frac{b_0}{r}, \\ A_1^+(r) &= \frac{r}{2}a_1 + \frac{b_1}{r}, \end{aligned}$$

where (a_0, b_0) and (a_1, b_1) are constants that are deduced from the boundary conditions of (19) and (21) respectively. Their expressions are given below:

$$\begin{aligned} a_0 &= 0 & \text{and} & & b_0 &= k, \\ a_1 &= \frac{k}{R_1} & \text{and} & & b_1 &= -\frac{kR_2^2}{2R_1}. \end{aligned}$$

Finally, the first asymptotic solutions have the following analytical form:

$$\begin{aligned} - \text{order 1: } & A_0^+(r) = \frac{k}{r}, \\ - \text{order 2: } & A_0^+(r) + \frac{\varepsilon}{\hat{\alpha}}A_1^+(r) = \frac{k}{r} + \frac{\varepsilon}{\hat{\alpha}}\left(\frac{k}{R_1}\frac{r}{2} - \frac{kR_2^2}{2R_1}\frac{1}{r}\right). \end{aligned}$$

4.2.3. *Analytical impedance solution.* We find the analytical expressions of A_1^ε by a simple integration of the first equations in Ω_0^m of the impedance model (23). The latter solution has the following general form:

$$(27) \quad A_1^\varepsilon(r) = \frac{r}{2}a_2^\varepsilon + \frac{b_2^\varepsilon}{r},$$

where a_2^ε and b_2^ε are constants that are deduced from the boundary conditions of (23). Their expressions are given below:

$$a_2^\varepsilon = \frac{\varepsilon}{\hat{\alpha}}\frac{2k}{\zeta^\varepsilon} \quad \text{and} \quad b_2^\varepsilon = k - a_2^\varepsilon\frac{R_2^2}{2}.$$

where $\zeta^\varepsilon = \left(\frac{\varepsilon}{\hat{\alpha}}(R_2^2 - R_1^2) + 2R_1\right)$.

5. NUMERICAL RESULTS

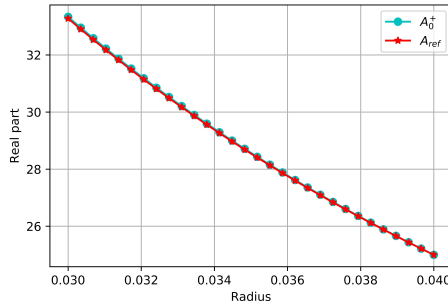
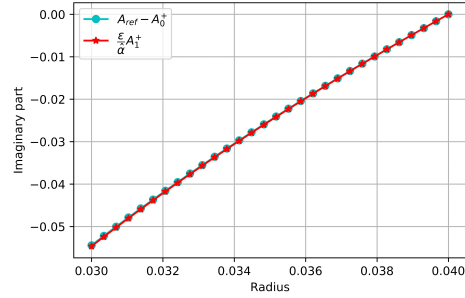
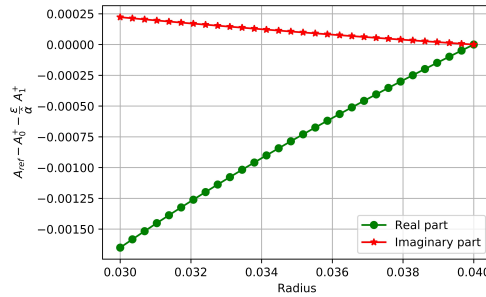
This section is devoted to establish numerical experiments concerning the above analytical solutions which have been implemented using Python 3 [19, 24]. The considered physical parameters are illustrated in Table 1. We choose arbitrarily small radius R_1 and R_2 . Moreover, the choice of the constant k , introduced in the Dirichlet condition (24), is also arbitrary.

Our numerical analysis follows the spirit of [2], where the finite element method was applied to demonstrate the accuracy of our asymptotic approach in a bi-dimensional setting for the eddy current problems in linear ferromagnetic materials. Indeed, the finite element solution was imposed as the reference solution in [2], since its corresponding analytical expression was not obvious to calculate.

First, we study the errors of orders one and two in the interval $[R_1, R_2]$ of the dielectric part Ω_0^m , in order to demonstrate the accuracy of our first asymptotic models.

Parameters	Value
Relative permeability (μ_r)	4000
Conductivity (σ)	2E+06 S/m
Frequency (f)	10 Hz
Inner radius (R_1)	0.03 m
Outer radius (R_2)	0.04 m
Skin depth (δ)	1.779E-03 m
Epsilon (ε)	1.41E-01
k	1

TABLE 1. Physical and numerical parameters

FIGURE 5. Real parts of A_0^+ and A_{ref} FIGURE 6. Imaginary parts of $A_{ref} - A_0^+$ and $\frac{\varepsilon}{\hat{\alpha}}A_1^+$ FIGURE 7. Real and Imaginary parts of the second order error $A_{ref} - A_0^+ - \frac{\varepsilon}{\hat{\alpha}}A_1^+$

In Figure 5, the real part of the first asymptotic A_0^+ is coherent with that of the reference solution in Ω_0^m denoted by A_{ref} . Moreover, we plot the error of the first order $A_{ref} - A_0^+$ and its correction $\frac{\varepsilon}{\hat{\alpha}}A_1^+$ for the imaginary parts in Figure 6. We remark that the corresponding graphs are approximately the same. Noting that we have the same results for the real parts. Thus, we

conclude that we have a good precision and correction of the first asymptotic solution. Since A_0^+ is real unlike A_{ref} , then it would be interesting to study the accuracy of the second order solution $A_0^+ + \frac{\varepsilon}{\hat{\alpha}} A_1^+$. This accuracy is established by the implementation of the second order error $A_{ref} - A_0^+ - \frac{\varepsilon}{\hat{\alpha}} A_1^+$. Indeed, Fig. 7 ensures that the real and imaginary parts of the latter error are small enough since they are less than 1%. As a consequence, we deduce the good approximation of the asymptotic solution $A_0^+ + \frac{\varepsilon}{\hat{\alpha}} A_1^+$.

Next, it is useful in power electronics to study the accuracy of our approach for different values of the physical parameters introduced in our work. In this context, we aim to compare the relative errors of the first asymptotic solutions with that of the impedance solution satisfying problem (23). We plot the convergence graphs with the log-log scale defining the following relative L_1^2 error:

$$Error = \frac{\|A_{ref} - A_{num}\|_{L_1^2([R_1, R_2])}}{\|A_{ref}\|_{L_1^2([R_1, R_2])}}$$

where the norm $\|\cdot\|_{L_1^2([R_1, R_2])}$ is defined as follows

$$\|u\|_{L_1^2([R_1, R_2])} = \left(\int_{[R_1, R_2]} |u|^2 r dr \right)^{\frac{1}{2}}.$$

Besides, A_{ref} is the reference solution in Ω_0^m , and A_{num} is the first asymptotic model A_0^+ , the second asymptotic model $A_0^+ + \frac{\varepsilon}{\hat{\alpha}} A_1^+$, or the impedance solution A_1^ε . We shall consider the case of varying relative magnetic permeabilities and frequencies as well. The geometry and the considered physical parameters are depicted in Figures 3-4, and Table 1. We recall that our work

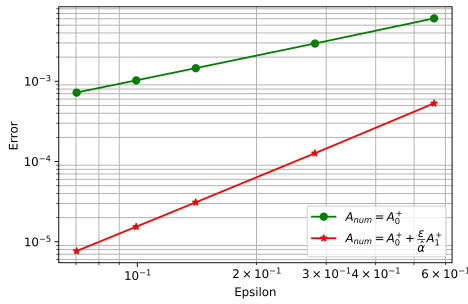


FIGURE 8. Relative L_1^2 error of the asymptotic solutions of order 1 and 2 for $f = 10$ Hz

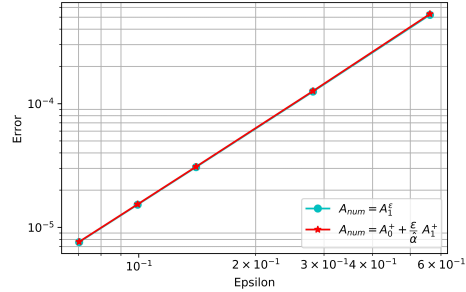


FIGURE 9. Relative L_1^2 error of the impedance solution and the second order model for $f = 10$ Hz

is restricted to eddy currents in linear ferromagnetic materials. In this regard, we suppose in Figures 8-9 that the relative magnetic permeabilities are

high and between 250 and 16000, and the frequency is 10 Hz. Noting that this latter range was chosen arbitrarily. We ensure in Figure 8 that when the small parameter ε decreases, the convergence rate of the relative L_1^2 error is of order 1 for the model A_0^+ and of order 2 for $A_0^+ + \frac{\varepsilon}{\hat{\alpha}} A_1^+$. Moreover, the asymptotic solution $A_0^+ + \frac{\varepsilon}{\hat{\alpha}} A_1^+$ provides an approximation to the reference solution which is of the same rate as the impedance solution A_1^ε , since the corresponding errors exhibited in Figure 9 behave in a similar manner with the variation of ε .

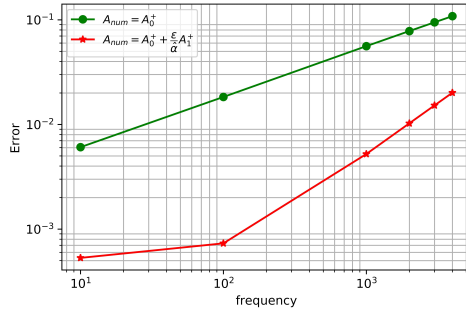


FIGURE 10. Relative L_1^2 error versus frequency for the asymptotic models for $\mu_r = 250$

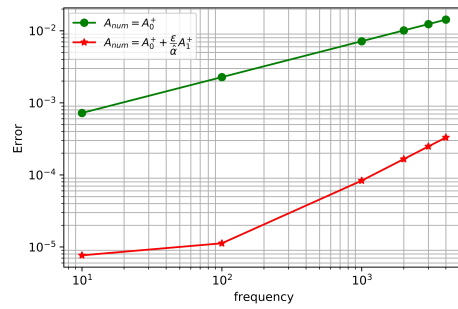


FIGURE 11. Relative L_1^2 error versus frequency for the asymptotic models for $\mu_r = 16000$

Now, the relative L_1^2 errors versus frequency for the asymptotic solutions are depicted in Figures 10-11 and for two different relative permeabilities. It is important to recall that our asymptotic approach is accomplished when the parameter $\varepsilon = \frac{1}{\mu_r \delta}$ is small i.e. less than one. In order to achieve this assumption, we must have the frequency between 10 Hz and 30 Hz, for $\mu_r = 250$, and between 10 Hz and 2 kHz for $\mu_r = 16000$. We will focus our analysis on these ranges of frequencies. On the one hand, when $\mu_r = 250$, the first order relative L_1^2 error is less than 1% for a range of frequencies between 10 Hz and 25 Hz. The range of frequencies becomes larger between 10 Hz and 1.6 kHz, when the relative permeability increases to 16000. On the other hand, we get slightly better results when the order of the asymptotic model is two. Indeed, the second order relative L_1^2 error is less than 1% for f in $[10, 30]$, when $\mu_r = 250$, and for a wider range of frequencies $[10, 2000]$ when $\mu_r = 16000$. It is worthwhile to note here that in both cases we remark a slope break for the graph corresponding to the second order error. Precisely, the slope is less important for low frequencies f in $[10, 100]$, so in the case of not enough "small" skin depth δ and when ε tends to zero, than that beyond this latter range of frequencies. As a future work, it could be interesting to

study the solution of higher order, for instance from 30 Hz on when $\mu_r \geq 250$, and from 2 kHz on when $\mu_r \geq 16000$ in order to get a relative L_1^2 error less than 1% for a deeper range of frequencies and when ε must be small as well.

6. CONCLUSION AND PERSPECTIVES

In conclusion, this paper provides efficient asymptotic models for axisymmetric eddy current problems in linear ferromagnetic materials. Our numerical experiments, established analytically for a special class of unbounded domains, confirm that the proposed asymptotic approach with two components suffices to ensure high accuracy for the case of low frequencies.

As a future work, we aim to study analytically and numerically the case of smooth and bounded geometries. Moreover, the multiscale approach for the three-dimensional eddy current problem as well as proofs of error estimates will be tackled in the PhD thesis [1] which is in preparation. It would be useful to expand our analysis numerically for the 3D case. Finally, we recall that our approach does not fit near edges and corners on the conductor interface. In this perspective, we will investigate in a forthcoming work an asymptotic procedure that provides reduced computational costs concerning geometrical singularities of the eddy current problems in linear ferromagnetic materials.

APPENDIX A. ELEMENTS OF DERIVATION FOR THE MULTISCALE EXPANSION

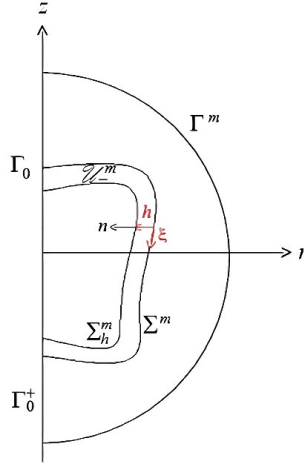
In this section, we will derive the terms of the asymptotic expansions introduced in (18) at any order $n \in \mathbb{N}$ as well as their governing equations having in mind that the orthoradial component of the magnetic vector potential $A = (A^+, A^-)$ satisfies the following problem

$$(28) \quad \begin{cases} DA^+ = 0 & \text{in } \Omega_0^m \\ DA^- - 2i\delta^{-2}A^- = 0 & \text{in } \Omega_-^m \\ BA^+ = \varepsilon\delta BA^- & \text{on } \Sigma^m, \\ A^+ = A^- & \text{on } \Sigma^m, \\ A^+ = g_\theta & \text{on } \Gamma^m \cup \Gamma_0^+, \end{cases}$$

and recalling that from notation 3, we deduce directly that the gauge conditions (3) in the cylindrical coordinates are satisfied. We remind that the magnetic potential A is concentrated on the boundary Σ^m and decays rapidly inside the conductor. Hence, it is convenient to use a local "normal coordinate system" in a tubular neighborhood \mathcal{U}_-^m of Σ^m inside Ω_-^m .

We denote by $(\vec{e}_r, \vec{e}_\theta, \vec{e}_z)$ the basis associated with the cylindrical coordinates (r, θ, z) . In the basis (\vec{e}_r, \vec{e}_z) , recall that $(r(\xi), z(\xi)) = \tau(\xi)$, $\xi \in (0, L)$ is an arc length coordinate on the interface Σ^m , and (ξ, h) is the associate normal coordinate system. The normal vector $n(\xi)$ at the point $\tau(\xi)$ writes

$$n(\xi) = (-z'(\xi), r'(\xi)).$$

FIGURE 12. A tubular neighborhood of Σ^m

Hence, the tubular neighborhood \mathcal{U}_-^m of Σ^m inside Ω_-^m is represented by the parameterization below

$$\mathcal{U}_-^m = \Psi(\mathbb{T}_L \times [0, h_0]),$$

where Ψ is the change of coordinates defined by

$$\Psi : (\xi, h) \mapsto (r, z),$$

noting that $r = r(\xi) - hz'(\xi)$, and $z = z(\xi) + hr'(\xi)$. Recalling that the curvature is defined by the following equality

$$k(\xi) = (r'z'' - z'r'')(\xi).$$

It is important to note that for $h_0 < \frac{1}{\|k\|_\infty}$, the change of coordinates Ψ is a C^∞ -diffeomorphism from the cylinder $\mathbb{T}_L \times [0, h_0)$ into \mathcal{U}_-^m . In contrast, when the radius of the interface curvature is very small, for example less than h , we get a rounded corner on Σ^m , and at the limit i.e. when the curvature is infinite we get a sharp corner (see for instance Remark 2 in [2]). In this paper, our interest lies in the case where the interface Σ^m is smooth. The latter cases are beyond the scope of this research.

In the following section, we aim to identify the profiles \mathfrak{A}_n as well as the asymptotic models A_n^+ introduced in (18) at any order $n \in \mathbb{N}$. To do that, we first expand the interior operator D and the boundary operator B in power series of the skin depth δ by applying the change of variables Ψ and the scaling $Y_3 = \frac{h}{\delta}$. Then we plug the resulting expressions in the problem (28). Finally, by identifying with the same power in ε , δ , and μ_r , we get the coefficients of the asymptotic expansion satisfying the family of boundary value problems at any order $n \in \mathbb{N}$. For the sake of simplicity, we will explicit the first asymptotics \mathfrak{A}_n and A_n^+ for $n = 0, 1$.

A.1. Expansion of the operators. In this part, we expand the operators D and B in the same manner as in [10].

Performing the change of the scaling $Y_3 = \frac{h}{\delta}$ and the change of variables Ψ , the interior operator D writes in coordinates (ξ, h) as

$$(29) \quad D = \delta^{-2} \left[\partial_{Y_3}^2 + \delta D_1 + \delta^2 R_\delta \right]$$

where $D_1(\xi, Y_3; \partial_\xi, \partial_{Y_3}) = -(k + \frac{z'}{r})(\xi) \partial_{Y_3}$ and R_δ is an operator, which has smooth coefficients in Y_3 and ξ , bounded in δ . Hence, we get

$$(30) \quad \delta^2 D = \sum_{n \geq 0} \delta^n C_n$$

where

$$\begin{aligned} C_0 &= \partial_{Y_3}^2, \\ C_1 &= -(k + \frac{z'}{r})(\xi) \partial_{Y_3}. \end{aligned}$$

Similarly, there holds $B = \delta^{-1} \partial_{Y_3} - \frac{z'}{r}(\xi)$ on the interface Σ .

A.2. Equations of the coefficients of the magnetic potential. In this section, we define $v_\delta(\xi, Y_3) = A^-(x)$ in \mathcal{U}_-^m . After the scaling $h \mapsto Y_3 = \frac{h}{\delta}$ in \mathcal{U}_-^m , the problem (28) writes

$$(31) \quad \begin{cases} DA^+ = 0 & \text{in } \Omega_0^m, \\ BA^+ = \varepsilon(\partial_{Y_3} - \frac{z'}{r})v_\delta & \text{on } \Sigma^m, \\ A^+ = 0 & \text{on } \Gamma^m \cup \Gamma_0^+, \end{cases}$$

and,

$$(32) \quad \begin{cases} (\partial_{Y_3}^2 - (\frac{1}{\hat{\alpha}})^2)v_\delta - \sum_{n \geq 1} \delta^n C_n v_\delta = 0 & \text{in } \mathbb{T}_L \times (0, +\infty), \\ v_\delta = A^+ & \text{on } \mathbb{T}_L \times \{0\}. \end{cases}$$

Now we plug the ansatz,

$$A^+ \sim \sum_{n \geq 0} \left(\frac{\varepsilon}{\hat{\alpha}}\right)^n A_n^+(x) \quad \text{in } \Omega_0^m,$$

and

$$v_\delta \sim \sum_{n \geq 0} \delta^n \mathfrak{A}_n(\xi, Y_3) \quad \text{in } \mathcal{U}_-^m,$$

with $\mathfrak{A}_n \rightarrow 0$ as $Y_3 \rightarrow +\infty$ in (31) and (32). Then by identification of terms in power of ε , δ and μ_r , the profiles \mathfrak{A}_n and A_n^+ satisfy the family of problems coupled by their conditions on the interface Σ^m

$$(33) \quad \begin{cases} DA_n^+ = 0 & \text{in } \Omega_0^m, \\ BA_n^+ = \hat{\alpha}(\delta_0^2)^{n-1}(\partial_{Y_3} \mathfrak{A}_{n-1} - \frac{z'}{r}(\xi) \mathfrak{A}_{n-2}) & \text{on } \Sigma^m, \\ A_n^+ = \delta_n^0 g_\theta & \text{on } \Gamma^m \cup \Gamma_0^+, \end{cases}$$

and

$$(34) \quad \begin{cases} \partial_{Y_3}^2 \mathfrak{A}_n - \left(\frac{1}{\hat{\alpha}}\right)^2 \mathfrak{A}_n = \sum_{p=1}^n C_p \mathfrak{A}_{n-p} & \text{in } \Sigma^m \times (0, +\infty), \\ \mathfrak{A}_n = \left(\frac{1}{\hat{\alpha}\delta_0^2}\right)^n A_n^+ & \text{in } \Sigma^m \times \{0\}, \end{cases}$$

where $\delta_0 = \sqrt{\frac{2}{\omega\sigma\mu_0}}$. In (33), δ_n^0 denotes the Kronecker symbol and we assume that $\mathfrak{A}_{-1} = \mathfrak{A}_{-2} = 0$. In the next section, we make explicit the first asymptotics (A_0^+, \mathfrak{A}_0) and (A_1^+, \mathfrak{A}_1) by induction.

A.3. First terms of the asymptotic expansion. For $n = 0$, we obtain that A_0^+ solves the problem below

$$(35) \quad \begin{cases} DA_0^+ = 0 & \text{in } \Omega_0^m, \\ BA_0^+ = 0 & \text{on } \Sigma^m, \\ A_0^+ = g_\theta & \text{on } \Gamma^m \cup \Gamma_0^+. \end{cases}$$

Then according to (35), \mathfrak{A}_0 solves the following ordinary differential equation (ODE)

$$(36) \quad \begin{cases} \partial_{Y_3}^2 \mathfrak{A}_0 - \left(\frac{1}{\hat{\alpha}}\right)^2 \mathfrak{A}_0 = 0 & \text{in } \Sigma^m \times (0, +\infty), \\ \mathfrak{A}_0 = A_0^+ & \text{on } \Sigma^m \times \{0\}. \end{cases}$$

Then the unique solution of (36) such that $\mathfrak{A}_0 \rightarrow 0$ as $Y_3 \rightarrow +\infty$ writes

$$(37) \quad \mathfrak{A}_0(\xi, Y_3) = A_0^+(\tau(\xi))e^{-\frac{Y_3}{\hat{\alpha}}}.$$

Next, for $n = 1$, we obtain A_1^+ from (37) that solves

$$(38) \quad \begin{cases} DA_1^+ = 0 & \text{in } \Omega_0^m, \\ BA_1^+ = -A_0^+ & \text{on } \Sigma^m, \\ A_1^+ = 0 & \text{on } \Gamma^m \cup \Gamma_0^+. \end{cases}$$

Then, according to (38), \mathfrak{A}_1 solves the following ODE

$$(39) \quad \begin{cases} \partial_{Y_3}^2 \mathfrak{A}_1 - \left(\frac{1}{\hat{\alpha}}\right)^2 \mathfrak{A}_1 = \frac{1}{\hat{\alpha}}\left(k + \frac{z'}{r}\right)(\xi)A_0^+ & \text{in } \Sigma^m \times (0, +\infty), \\ \mathfrak{A}_1 = \frac{1}{\hat{\alpha}\delta_0^2}A_1^+ & \text{on } \Sigma^m \times \{0\}. \end{cases}$$

Then the unique solution of (39) such that $\mathfrak{A}_1 \rightarrow 0$ as $Y_3 \rightarrow +\infty$ writes

$$(40) \quad \mathfrak{A}_1(\xi, Y_3) = \left[\frac{1}{\hat{\alpha}\delta_0^2}A_1^+(\tau(\xi)) - \frac{Y_3}{2}\left(k + \frac{z'}{r}\right)(\xi)A_0^+(\tau(\xi)) \right] e^{-\frac{Y_3}{\hat{\alpha}}}.$$

APPENDIX B. ELEMENTS OF PROOFS OF THE ANALYTICAL SOLUTIONS

In this section, we will perform the same procedure as in [4] in order to calculate our analytical solutions (25), (26), and (27). We recall that the electric current flows in the \vec{e}_θ direction and that is uniformly distributed in

the \vec{e}_z direction. Then it results the following expressions of the operators D and B (see for instance (13)):

$$(41) \quad \begin{aligned} D(r, z; \partial_r, \partial_z) &= \partial_r^2 + \frac{1}{r}\partial_r - \frac{1}{r^2}, \\ B(\xi; \partial_r, \partial_z) &= -\partial_r - \frac{1}{r}. \end{aligned}$$

Noting that, in our cylindrical case, we have $z'(\xi) = 1$ and $r'(\xi) = 0$. Equivalently, we get the following expressions of the operators

$$(42) \quad \begin{aligned} D(r, z; \partial_r, \partial_z)(\cdot) &= \partial_r \left(\frac{1}{r} (\partial_r (r \cdot)) \right), \\ B(\xi; \partial_r, \partial_z)(\cdot) &= - \left(\frac{1}{r} (\partial_r (r \cdot)) \right). \end{aligned}$$

In the following, we will calculate by order the analytical value of $A = (A^+; A^-)$, A_0^+ , A_1^+ and A_1^ε . Taking into account that we only have one connected component and according to (42), the first and second equations of the problem (28) become

$$(43) \quad \partial_r \left(\frac{1}{r} (\partial_r (r A^+)) \right) (r) = 0 \quad \text{if } R_1 < r < R_2,$$

$$(44) \quad -\partial_r \left(\frac{1}{r} (\partial_r (r A^-)) \right) (r) + i\omega\sigma\mu_r\mu_0 A^- = 0 \quad \text{if } 0 < r < R_1,$$

with boundary conditions

$$(45) \quad A^-(r) \text{ is bounded as } r \rightarrow 0,$$

$$(46) \quad A^+(r) = \frac{k}{r} \quad \text{if } r = R_2.$$

Moreover, we have the following transmission conditions

$$(47) \quad A^-(R_1) = A^+(R_1),$$

$$(48) \quad \frac{1}{r} (\partial_r (r A^-)) (R_1) = \mu_r \frac{1}{r} (\partial_r (r A^+)) (R_1).$$

Consequently, the model consists of equations (43), (44) with boundary conditions (45), (46) and interface conditions (47), (48). Simple integration of equation (43) yields to the following form

$$(49) \quad A^+(r) = \frac{r}{2}a + \frac{b}{r},$$

where a , b and c are constants. Now, in order to solve equation (44), we perform the change of variable $x = r\gamma$, in $(0, R_1)$, where $\gamma = \sqrt{\omega\sigma\mu_r\mu_0}e^{i\frac{\pi}{4}}$. Then, we get

$$(50) \quad x^2 \partial_x^2 \tilde{A}^- + x \partial_x \tilde{A}^- - (x^2 + 1)\tilde{A}^- = 0 \quad \text{in } (0, R_1),$$

where $\tilde{A}^-(x) = A^-\left(\frac{x}{\gamma}\right)$. Equation (50) is a Bessel equation for which its general equation is given by

$$(51) \quad \tilde{A}^-(x) = c\mathcal{I}_1(x) + d\mathcal{K}_1(x),$$

where \mathcal{I}_1 and \mathcal{K}_1 are the modified Bessel functions of the first and second kind respectively [27, Chapter 10 - pages 248–250]. By using the boundary condition (45), we deduce that $d = 0$. On the other hand, the transmission conditions (47) and (48), and the boundary condition (46) imply the system below

$$(52) \quad \begin{cases} c\mathcal{I}_1(\gamma R_1) = \frac{R_1}{1}a + \frac{b}{R_1}, \\ c[\gamma\mathcal{I}'(\gamma R_1) + \mathcal{I}_1(\gamma R_1)] = \mu_r R_1 a, \\ \frac{R_2}{2}a + \frac{b}{R_2} = \frac{k}{R_2}. \end{cases}$$

Thus, we obtain a linear system of order three for constant unknowns a , b and c . Solving this linear system, we get

$$\begin{aligned} a &= \frac{k}{R_1} \frac{g_1}{g_2}, \\ b &= k - a \frac{R_2^2}{2}, \\ c &= [\mathcal{I}_1^{-1}(\gamma R_1) \frac{(R_1^2 - R_2^2)}{2R_1}] a + \frac{k}{R_1} \mathcal{I}_1^{-1}(\gamma R_1). \end{aligned}$$

Noting that g_1 and g_2 are constants defined as follows

$$\begin{aligned} g_1 &= \mathcal{I}_1(\gamma R_1) + \gamma R_1 \mathcal{I}'_1(\gamma R_1), \\ g_2 &= R_1 \mu_r \mathcal{I}_1(\gamma R_1) - g_1 \frac{(R_1^2 - R_2^2)}{2R_1}. \end{aligned}$$

In a similar manner, we calculate next the analytical values of A_0^+ , A_1^+ and A_1^ε . We recall that A_0^+ satisfies the following problem

$$(53) \quad \begin{cases} \partial_r \left(\frac{1}{r} (\partial_r (r A_0^+)) \right) (r) = 0, & \text{if } R_1 < r < R_2, \\ -\frac{1}{r} (\partial_r (r A_0^+)) (r) = 0 & \text{if } r = R_1 \\ A_0^+ = \frac{k}{r} & \text{if } r = R_2. \end{cases}$$

By a simple integration of the first equation of (53), we get the following form

$$(54) \quad A_0^+(r) = \frac{r}{2} a_0 + \frac{b_0}{r},$$

where a_0 and b_0 are constants that are deduced from the boundary conditions and satisfies the linear system of order two below

$$(55) \quad \begin{cases} -a_0 = 0, \\ \frac{R_2}{2}a_0 + \frac{b_0}{R_2} = \frac{k}{R_2}. \end{cases}$$

Solving the system (55), we get

$$a_0 = 0 \quad \text{and} \quad b_0 = k.$$

Hence we deduce that

$$(56) \quad A_0^+(r) = \frac{k}{r}.$$

Similarly, according to (21) and the expression of A_0^+ in (56), A_1^+ solves the following system

$$(57) \quad \begin{cases} \partial_r \left(\frac{1}{r} (\partial_r (r A_1^+)) \right) (r) = 0 & \text{if } R_1 < r < R_2, \\ -\frac{1}{r} (\partial_r (r A_1^+)) (r) = -\frac{k}{r} & \text{if } r = R_1, \\ A_1^+(r) = 0 & \text{if } r = R_2. \end{cases}$$

By a simple integration of the first equation of the above system (57), A_1^+ satisfies

$$(58) \quad A_1^+(r) = \frac{r}{2}a_1 + \frac{b_1}{r}$$

where a_1 and b_1 solves the following linear system deduced from the boundary conditions in (57):

$$(59) \quad \begin{cases} -a_1 = -\frac{k}{R_1}, \\ \frac{R_2}{2}a_1 + \frac{b_1}{R_2} = 0. \end{cases}$$

Solving this linear system, we get the constants a_1 and b_1 as follows

$$a_1 = \frac{k}{R_1} \quad \text{and} \quad b_1 = -\frac{kR_2^2}{2R_1}.$$

As a consequence, the second order asymptotic solution in its analytical form writes

$$(60) \quad A_0^+(r) + \frac{\varepsilon}{\hat{\alpha}} A_1^+ = \frac{k}{r} + \frac{\varepsilon}{\hat{\alpha}} \left(\frac{k}{R_1} \frac{r}{2} - \frac{kR_2^2}{2R_1} \frac{1}{r} \right).$$

Finally, the impedance solution A_1^ε satisfying (23) is calculated in a similar way as the first asymptotics A_0^+ and A_1^+ .

ACKNOWLEDGEMENTS

Authors express their gratitude to Ronan PERRUSSEL for his useful remarks and discussions concerning the numerical part.

REFERENCES

- [1] D. Abou El Nasser El Yafi. *Résolution numérique des équations de diffusion dans des matériaux ferromagnétiques*. PhD thesis, Université de Pau et des pays de l'Adour, *In preparation*.
- [2] D. Abou El Nasser El Yafi, V. Péron, R. Perrussel, and L. Krähenbühl. Numerical study of the magnetic skin effect: Efficient parameterization of 2d surface-impedance solutions for linear ferromagnetic materials. *International Journal of Numerical Modelling: Electronic Networks, Devices and Fields*, pages 30–51, 2022.
- [3] F. Assous, P. Ciarlet Jr, and S. Labrunie. Solution of axisymmetric maxwell equations. *Mathematical methods in the applied sciences*, 26(10):861–896, 2003.
- [4] A. Bermúdez, D. Gómez, M. C. Muñoz, and P. Salgado. Transient numerical simulation of a thermoelectrical problem in cylindrical induction heating furnaces. *Advances in computational mathematics*, 26(1):39–62, 2007.
- [5] C. Bernardi, M. Dauge, Y. Maday, and M. Azaïez. *Spectral methods for axisymmetric domains*, volume 3. Editions Scientifiques Et, 1999.
- [6] O. Bíró. Edge element formulations of eddy current problems. *Computer methods in applied mechanics and engineering*, 169(3-4):391–405, 1999.
- [7] A. Bossavit. *Electromagnetisme, en vue de la modélisation*, volume 14. Springer Science & Business Media, 2004.
- [8] A. Buffa, H. Ammari, and J.-C. Nédélec. A justification of eddy currents model for the maxwell equations. *SIAM Journal on Applied Mathematics*, 60(5):1805–1823, 2000.
- [9] F. Buret, M. Dauge, P. Dular, L. Krahenbuhl, V. Péron, R. Perrussel, C. Poignard, and D. Voyer. Eddy currents and corner singularities. *IEEE transactions on magnetics*, 48(2):679–682, 2012.
- [10] G. Caloz, M. Dauge, E. Faou, and V. Péron. On the influence of the geometry on skin effect in electromagnetism. *Computer Methods in Applied Mechanics and Engineering*, 200(9-12):1053–1068, 2011.
- [11] P. Ciarlet and S. Labrunie. Numerical solution of maxwell's equations in axisymmetric domains with the fourier singular complement method. *Journal of Difference Equations and Applications*, 3:113–155, 2011.
- [12] M. Costabel, M. Dauge, and S. Nicaise. Singularities of eddy current problems. *ESAIM: Mathematical Modelling and Numerical Analysis*, 37(5):807–831, 2003.
- [13] M. Dauge, P. Dular, L. Krähenbühl, V. Péron, R. Perrussel, and C. Poignard. Corner asymptotics of the magnetic potential in the eddy-current model. *Mathematical Methods in the Applied Sciences*, 37(13):1924–1955, 2014.
- [14] M. Dauge, E. Faou, and V. Péron. Comportement asymptotique à haute conductivité de l'épaisseur de peau en électromagnétisme. *Comptes Rendus Mathématique*, 348(7-8):385–390, 2010.
- [15] P. Dular. *Modélisation du champ magnétique et des courants induits dans des systèmes tridimensionnels non linéaires*. PhD thesis, ULiège-Université de Liège, 1994.
- [16] P. Dular, V. Péron, R. Perrussel, L. Krähenbühl, and C. Geuzaine. Perfect conductor and impedance boundary condition corrections via a finite element subproblem method. *IEEE transactions on magnetics*, 50(2):29–32, 2014.
- [17] H. Haddar, P. Joly, and H.-M. Nguyen. Generalized impedance boundary conditions for scattering problems from strongly absorbing obstacles: The case of maxwell's equations. *Mathematical Models and Methods in Applied Sciences*, 18(10):1787–1827, 2008.
- [18] S. Hariharan and R. MacCamy. Integral equation procedures for eddy current problems. *Journal of Computational Physics*, 45(1):80–99, 1982.
- [19] D. Hellmann. *The Python standard library by example*. Addison-Wesley Upper Saddle River, USA, 2011.

- [20] R. Hiptmair. Symmetric coupling for eddy current problems. *SIAM Journal on Numerical Analysis*, 40(1):41–65, 2002.
- [21] M. Issa, J.-R. Poirier, R. Perrussel, O. Chadebec, and V. Péron. Boundary element method for 3d conductive thin layer in eddy current problems. *COMPEL-The international journal for computation and mathematics in electrical and electronic engineering*, 38(2):502–521, 2019.
- [22] L. Krahenbuhl and D. Muller. Thin layers in electrical engineering-example of shell models in analysing eddy-currents by boundary and finite element methods. *IEEE Transactions on Magnetics*, 29(2):1450–1455, 1993.
- [23] M. Leontovich. Approximate boundary conditions for the electromagnetic field on the surface of a good conductor. *Investigations on radiowave propagation*, 2:5–12, 1948.
- [24] M. Lutz. *Learning python: Powerful object-oriented programming*. O’Reilly Media, Inc., 2013.
- [25] R. MacCamy and E. Stephan. Solution procedures for three-dimensional eddy current problems. *Journal of mathematical analysis and applications*, 101(2):348–379, 1984.
- [26] R. C. MacCamy and E. Stephan. A skin effect approximation for eddy current problems. In *Analysis and Thermomechanics*, pages 175–186. Springer, 1987.
- [27] F. W. Olver, D. W. Lozier, R. F. Boisvert, and C. W. Clark. *NIST handbook of mathematical functions*. Cambridge university press, 2010.
- [28] V. Péron. *Modélisation mathématique de phénomènes électromagnétiques dans des matériaux à fort contraste*. PhD thesis, Université Rennes 1, 2009.
- [29] V. Péron. Asymptotic models and impedance conditions for highly conductive sheets in the time-harmonic eddy current model. *SIAM Journal on Applied Mathematics*, 79(6):2242–2264, 2019.
- [30] V. Péron and C. Poignard. On a magnetic skin effect in eddy current problems: the magnetic potential in magnetically soft materials. *Zeitschrift für angewandte Mathematik und Physik*, 72(4):1–19, 2021.
- [31] R. Perrussel and C. Poignard. Asymptotic expansion of steady-state potential in a high contrast medium with a thin resistive layer. *Applied Mathematics and Computation*, 221:48–65, 2013.
- [32] A. A. Rodríguez and A. Valli. *Eddy Current Approximation of Maxwell Equations: Theory, Algorithms and Applications*, volume 4. Springer Science & Business Media, 2010.
- [33] S. Rytov. Calcul du skin-effect par la méthode des perturbations. *J. Phys. USSR*, 2(3):233–242, 1940.
- [34] K. Schmidt and A. Chernov. A unified analysis of transmission conditions for thin conducting sheets in the time-harmonic eddy current model. *SIAM Journal on Applied Mathematics*, 73(6):1980–2003, 2013.
- [35] E. Stephan. Solution procedures for interface problems in acoustics and electromagnetics. In *Theoretical acoustics and numerical techniques*, pages 291–348. Springer, 1983.

Dima ABOU EL NASSER EL YAFI, Victor PÉRON
 Laboratoire de mathématiques appliquées de Pau, E2S UPPA, CNRS
 Université de Pau et des pays de l’Adour
 64000 Pau
 France
 E-mails: dima.abou-el-nasser-el-yafi@univ-pau.fr; victor.peron@univ-pau.fr